Geodesic acoustic mode oscillation in the low frequency rangea)

T. Watari, Y. Hamada, T. Notake, N. Takeuchi, and K. Itoh

Citation: Physics of Plasmas (1994-present) **13**, 062504 (2006); doi: 10.1063/1.2206170
View online: http://dx.doi.org/10.1063/1.2206170
View Table of Contents: http://scitation.aip.org/content/aip/journal/pop/13/6?ver=pdfcov
Published by the AIP Publishing

Geodesic acoustic mode oscillation in the low frequency range[a)]

T. Watari, Y. Hamada, T. Notake, N. Takeuchi, and K. Itoh
National Institute for Fusion Science, 322-6, Oroshi-cho, Toki-city, Gifu, Japan

(Received 21 July 2005; accepted 27 April 2006; published online 7 June 2006)

In order to understand the various appearances of geodesic acoustic modes (GAM) in experiments, the following specific problems are theoretically addressed: (1) The asymmetry of the potential field of GAMs, which is enhanced by the coupling with ion acoustic modes. It may affect GAMs in plasmas with electron temperatures higher than those of the ions. (2) The possible existence of GAMs in the lower frequency range: This is discussed in connection with the uniqueness of the kinetic response of the plasma to an external field associated with the geodesic curvature of the magnetic lines of force. (3) The extension of the theory to cover both tokamaks and helical systems: Differences between the helical-type and the tokamak-type GAMs are discussed in terms of their differences in connection length. In a device of mixed helicity, helical natured GAMs are predicted to appear depending on the intensity of the corresponding geodesic curvature and electron temperature. © *2006 American Institute of Physics*. [DOI: 10.1063/1.2206170]

I. INTRODUCTION

[1]Since plasma drifts with the velocity $\vec{E}\times\vec{B}$, the rotation speed of the plasma is related to the radial electric field E_r. The rotating plasma is provided with a restoring force by the geodesic curvature of the magnetic lines of forces, which exist intrinsically in tori. Therefore, the plasmas are subject to oscillatory motions, the existence of which was theoretically suggested by Winsor*et al.*[1] This oscillation is referred to as the geodesic acoustic mode (GAM) according to the origin of the restoring force. The physics of GAM oscillation has been studied initially using magnetohydrodynamic (MHD) equations and applied in a limited way to tokamaks.[2–4] In recent investigations, such rotations of the plasma have also been found in many simulations, and they are believed to be driven by plasma turbulence.[5–13] The sheared flow are shown in turn to regulate transport[14,15] and thus they are attracting more and more attention. Due to progress in diagnostics, evidence of sheared zonal flows including GAMs has been observed in experiments.[16–26]

Progress in the physics of flow drive and the regulation of the turbulence have been reviewed, for instance, in Refs. 27 and 28. The mechanism of the generation of the radial electric field is in itself an interesting subject of research. It is believed that zonal flows with frequencies lower than GAMs, which are referred to as stationary zonal flows, have lower viscosity.[29–31] Therefore, they may play a larger role in regulating the turbulence.

Experimental papers[16–26] reported various appearances of GAM oscillations and many questions have arisen: (1) The GAM oscillations are found only in limited regions of the plasma in some devices, such as the doublet-IIID (D-IIID),[16] the Axisymmetric Diverter Experiment (ASDEX-U),[25] and the Japan Atomic Energy Research Institute Fusion Toru Modified (JFT-IIM),[21] while GAM is found in a wider domain in the plasmas in the Texas Experimental Tokamak (TEXT),[17,18] the Japanese Institute of Plasma Physics Tokamak (JIPP T-U),[19,20] the Tokamak-10 (T-10),[26] and the compact helical system (CHS).[22] (2) The GAM is found also in the helical system CHS and its theoretical basis has to be developed. (3) An up-down asymmetry of the plasma density is predicted by theory, yet it has not been clearly detected in the experiments. (4) More than two branches of GAM-like oscillations are reported in the experimental papers: GAM-like oscillations are found in two frequencies in ASDEX-U and JIPP-TII U and more than two are found in CHS.

In order to reach a full understanding of the GAM, it is necessary to reconsider as well as to conduct further experimental investigations. Particularly, the prediction of the parameter range where GAMs exist may be useful because it facilitates a comparison between the theory and experimental results. In revising the theory, we will address how the GAM is modified in kinetic description by its coupling with sound waves. The foregoing MHD-based theories suggest that it will cause a frequency shift,

$$\delta\omega^2 = \omega^2 - \omega_{G,\mathrm{MHD}}^2 = k_\parallel^2 c_s^2, \tag{1}$$

over the ordinary GAM frequency $\omega_{G,\mathrm{MHD}}^2 \approx 2[T_e + (5/3)T_i]/m_i(1/R^2)$ (see, for example, Refs. 2 and 27). The term on the right-hand side is regarded as parallel dynamics correction and assumes a form $c_s^2 \equiv (\xi_1 T_i + \xi_2 T_e)/m_i$ with ξ_1 and ξ_2 being numbers of order unity. However, these terms can be correctly evaluated only with a kinetic approach.

Most simply interpreted, a GAM is an oscillating plasma rotation in response to the uniform ($m=0$, $n=0$) potential field. However, parallel dynamics plays an important role in determining the associated nonuniformity of the potential field. An expression measuring the nonuniformity is given in this paper as well as a suggestion that it plays a significant role beyond shifting the GAM frequency perturbatively.

We will also study the lower frequency range

[a)]This paper is based on a presentation at the IAEA Technical Meeting on the Theory of Plasma Instabilities, Trieste, Italy, 2–4 March 2005.

$(\omega^2 < \omega_{G,\mathrm{MHD}}^2)$ in search of a new branch of GAM. If there is such a mode with a high quality factor, it will effectively regulate the drift wave turbulences in the low frequency range.[15] Due to the complexity of the response of the plasma in kinetic analyses, there is a possibility that a GAM-like mode is found around the frequency

$$\omega \sim k_{\|} v_{T,i} = v_{T,i}/Rq = \sqrt{2T_i/m_i}/Rq, \tag{2}$$

lower than $\omega_{G,\mathrm{MHD}}$ by a factor of $1/q$. It will fall in the low frequency edge of the turbulence, where drift waves condensate due to inverse cascade processes and are finally dissipated. Therefore, the properties of this mode are important in determining the spectrum of the turbulence and thus in determining transport, even if the mode has a low quality factor.

This paper is organized as follows: In Sec. II, the dispersion relation of the GAM oscillation is formulated, clarifying in Sec. II A the approximation used, giving special attention in Sec. II B to the roles of the nonuniform field, and giving in Sec. II C the dispersion relation of the GAM on which the discussions in the following sections are made. In Sec. III, the revised theory is applied to tokamaks. deriving in Sec. III A a reduced form and applying it in Sec. III B to the two typical cases of $T_e/T_i=1$ and $T_e/T_i>1$. In Sec. III C, the results obtained in Sec. III B are given interpretations from the point of view of the intervention of the sound waves in the GAM mechanism. In Sec. IV, the theory is applied to helical systems, including straight (Sec. IV A) and toroidal (Sec. IV B) helical systems. In the latter, a possible coexistence of tokamak-type and helical-type GAMs is noted according to the relative intensity of the ripples in their magnetic field, if $T_e/T_i>1$. In Sec. V, the damping rates of the modes in the GAM frequency range are studied using the dispersion relation in a full complex analysis. In Sec. VI, the applicability range of results obtained in this paper is discussed, and the problems to be solved are suggested. Conclusions are presented in Sec. VII.

II. BASIC EQUATIONS

A. Formulation and clarification of assumptions

The extension of GAM theory to helical systems has been addressed in our previous paper,[32] where it was found that the helical geodesic curvature of the magnetic field is the cause of the geodesic acoustic mode. Therefore, the flux coordinate has been introduced with poloidal and toroidal coordinates (θ,ζ) on which a Fourier expansion of the magnetic field intensity is made:

$$B = B_0\left(1 + \sum_{m,n} \delta_{m,n}(\psi)\cos(m\theta - n\zeta)\right), \tag{3}$$

where ψ is the poloidal flux used as the flux surface label and m,n are the poloidal and toroidal mode numbers of the confining magnetic field. The drift kinetic equation is solved with a drift velocity of the particles $\vec{v}_D$ expressed in terms of $\delta_{m,n}(\psi)$; the latter is associated with the curvature of the magnetic lines of force:

$$\frac{\partial f_1}{\partial t} + (\vec{v}_{\|} + \vec{v}_D)\cdot\vec{\nabla} f_1 + \{-e(\vec{v}_{\|} + \vec{v}_D) \cdot \vec{\nabla}[(\phi - \langle\phi\rangle) + \langle\phi\rangle]\}\frac{\partial f_0}{\partial w} = 0. \tag{4}$$

Electrons and ions are not distinguished in Sec. II A, because their motions are subject to the same equation. Based on the straight magnetic field line coordinate (θ,ζ,ψ), $\vec{v}_D$ in Eq. (4) is written as follows:

$$\vec{v}_D\cdot\vec{\nabla}\psi = \frac{2Tc}{eB_0}\left(\frac{m v_{\|}^2 + \frac{1}{2}m v_{\perp}^2}{2T}\right)\alpha_{m,n}\sin(m\theta - n\zeta) = v_T\left(\frac{v_T}{\omega_{c,0}}\right)\gamma\alpha_{m,n}\sin(m\theta - n\zeta), \tag{5}$$

with

$$\alpha_{m,n} \equiv \alpha_{m,n}(\psi) = \frac{1}{\sqrt{g}B^2}2\pi B_0(mB_\zeta + nB_\theta)\delta_{m,n}(\psi) = 2\pi\frac{(mB_\zeta + nB_\theta)}{qB_\zeta + B_\theta}B_0\delta_{m,n}(\psi) \tag{6}$$

and

$$\gamma = \left(\frac{m v_{\|}^2 + \frac{1}{2}m v_{\perp}^2}{2T}\right). \tag{7}$$

Here, B_ζ and B_θ are the covariant components of the toroidal and poloidal magnetic field, which are flux functions in Boozer coordinates. $\sqrt{g}$ is the Jacobean. We specify the coordinate to be Boozer coordinates $(\sqrt{g}\propto B^{-2})$, so that $\alpha_{m,n}=\alpha_{m,n}(\psi)$ is a flux function. We separate the distribution functions into two parts and seek their solutions: $f_1(U\rightarrow)$, the perturbation caused by the uniform potential field $\langle\phi\rangle$ and $f_1(NU\rightarrow)$, the part caused by the nonuniform field $(\phi-\langle\phi\rangle)$. $\langle A\rangle$ is the flux surface average of the quantity A:

$$\frac{\partial f_1(U\rightarrow)}{\partial t} + (\vec{v}_{\|})\cdot\vec{\nabla} f_1(U\rightarrow) = \{e(\vec{v}_{\|} + \vec{v}_D)\cdot\vec{\nabla}[\langle\phi\rangle]\}\frac{\partial f_0}{\partial w} \tag{8}$$

and

$$\frac{\partial f_1(NU\rightarrow)}{\partial t} + (\vec{v}_{\|} + \vec{v}_D)\cdot\vec{\nabla} f_1(NU\rightarrow) = \{e(\vec{v}_{\|} + \vec{v}_D)\cdot\vec{\nabla}[\phi - \langle\phi\rangle]\}\frac{\partial f_0}{\partial w}. \tag{9}$$

Here we introduce $\tilde{\phi}_s$, $\tilde{\phi}_c$, and $\tilde{\phi}_0$ by

$$(\phi - \langle\phi\rangle) = (\tilde{\phi}_s\sin\theta + \tilde{\phi}_c\cos\theta)\exp(-i\omega t + ik_\psi\psi),$$

$$\langle\phi\rangle = \tilde{\phi}_0\exp(-i\omega t + ik_\psi\psi). \tag{10}$$

Similarly, we decompose the caused nonuniform distribution function $f(\rightarrow NU)$ defining $\tilde{f}_s(\rightarrow NU)$ and $\tilde{f}_c(\rightarrow NU)$ in the following equation:

$$f(\rightarrow NU) = \{[\tilde{f}_s(\rightarrow NU)\sin\theta] + [\tilde{f}_c(\rightarrow NU)\cos\theta]\} \times \exp(-i\omega t + ik_\psi \psi). \tag{11}$$

Equations (8) and (9) have the operators $(\vec{v}_\parallel + \vec{v}_D)\cdot\vec{\nabla} f_1$ on the left-hand side. These terms are known to create harmonics due to the spatial variation of both $\vec{v}_\parallel$ and $\vec{v}_D$. Since they have single-parameter dependences on time t through the spatial dependence on (θ, ζ), their variations have to be considered simultaneously. A more detailed consideration of this problem is introduced in Ref. 33. For this paper, however, the constancy of $\vec{v}_\parallel$ is assumed and $\vec{v}_D$ is ignored with respect to the former. The equation is then simplified with the use of the following transformations:

$$\vec{v}_\parallel \cdot \vec{\nabla} \cos(m\theta - n\zeta) \approx -k_{\parallel,m,n} v_\parallel \sin(m\theta - n\zeta), \tag{12}$$

$$\vec{v}_\parallel \cdot \vec{\nabla} \sin(m\theta - n\zeta) \approx k_{\parallel,m,n} v_\parallel \cos(m\theta - n\zeta), \tag{13}$$

where

$$k_{\parallel,m,n} \equiv (mB^\theta - nB^\zeta)/B$$

with B^θ and B^ζ the contravariant components of the magnetic field. We also assume that $K_{\parallel,m,n}$ is independent of (θ, ζ), though it is correct only to the first order in $\delta_{m,n}$ on the Boozer coordinates.

Using these assumptions, we obtain

$$\begin{pmatrix} -i\omega & k_{\parallel,m,n} v_\parallel \\ k_{\parallel,m,n} v_\parallel & -i\omega \end{pmatrix} \begin{pmatrix} \tilde{f}_s(U \rightarrow NU) \\ \tilde{f}_c(U \rightarrow NU) \end{pmatrix} = \beta_{m,n} \frac{f_0}{T} \tilde{\phi}_0 \begin{pmatrix} 1 \\ 0 \end{pmatrix},$$

$$\beta_{m,n} = v_\perp \left(\frac{v_T}{\omega_{c,0}} k_\psi \right) \alpha_{m,n} \gamma,$$

$$\gamma = \left(x_\parallel^2 + \frac{1}{2} x_\perp^2 \right), \tag{14}$$

where $x_\parallel = v_\parallel / v_T$ and $x_\perp = v_\perp / v_T$ with $v_T = \sqrt{2T/m}$. The arrow in the bracket $(U \rightarrow NU)$ indicates that the induced nonuniform perturbation is due to a uniform potential field. Solutions are obtained to the first order in $(v_T / \omega_{c,0} k_\psi)$ taking the following forms:

$$\tilde{f}_s(U \rightarrow NU) = -\frac{1}{2}\frac{1}{T} v_\perp \left(k_\psi \frac{v_T}{\omega_{c,0}} \right) \alpha_{m,n} \tilde{\phi}_0 \gamma \left(\frac{1}{\omega - (k_{\parallel,m,n} v_\parallel)} + \frac{1}{\omega + (k_{\parallel,m,n} v_\parallel)} \right) f_0,$$

$$\tilde{f}_c(U \rightarrow NU) = i(k_{\parallel,m,n} v_\parallel / \omega) \tilde{f}_s. \tag{15}$$

Similarly, the nonuniform distribution functions $\tilde{f}_s(NU \rightarrow NU)$ and the distribution functions due to the nonuniform potential field $\tilde{f}_c(NU \rightarrow NU)$ are obtained from the following equations, which are derived from Eq. (9):

$$\begin{pmatrix} -i\omega & -k_{\parallel,m,n} v_\parallel \\ k_{\parallel,m,n} v_\parallel & -i\omega \end{pmatrix} \begin{pmatrix} \tilde{f}_s(NU \rightarrow NU) \\ \tilde{f}_c(NU \rightarrow NU) \end{pmatrix} = \frac{-e}{T} f_0 \begin{pmatrix} -k_{\parallel,m,n} v_\parallel \tilde{\phi}_c \\ k_{\parallel,m,n} v_\parallel \tilde{\phi}_s \end{pmatrix}. \tag{16}$$

The solution is obtained in the following way:

$$\tilde{f}_s(NU \rightarrow NU) = -\frac{e}{T}\tilde{\phi}_s f_0 + \frac{\omega}{2}\left(\frac{1}{\omega - (k_{\parallel,m,n} v_\parallel)} + \frac{1}{\omega + k_{\parallel,m,n} v_\parallel} \right) \frac{e}{T} f_0 \tilde{\phi}_s + i\frac{\omega}{2}\left(\frac{1}{\omega - (k_{\parallel,m,n} v_\parallel)} - \frac{1}{\omega + k_{\parallel,m,n} v_\parallel} \right) \frac{e}{T} f_0 \tilde{\phi}_c \tag{17}$$

and

$$\tilde{f}_c(NU \rightarrow NU) = -\frac{e}{T}\tilde{\phi}_c f_0 + \frac{\omega}{2}\left(\frac{1}{\omega - (k_{\parallel,m,n} v_\parallel)} + \frac{1}{\omega + k_{\parallel,m,n} v_\parallel} \right) \frac{e}{T} \tilde{\phi}_c f_0 - i\frac{\omega}{2}\left(\frac{1}{\omega - (k_{\parallel,m,n} v_\parallel)} - \frac{1}{\omega + k_{\parallel,m,n} v_\parallel} \right) \frac{e}{T} f_0 \tilde{\phi}_s. \tag{18}$$

B. Determination of the nonuniform field

In determining the nonuniform field, we use quasineutrality. This scheme of calculation has been explored by Lebedev *et al.*[34] and was extended to helical systems in a recent work by Sugama *et al.*[35] The sine and cosine components of the density perturbation due to the nonuniform field are obtained by integrating Eqs. (17) and (18):

$$4\pi e n_c(NU \rightarrow NU) = -k_D^2 [1 + \zeta_{m,n} Z_p(\zeta_{m,n})] \tilde{\phi}_c \times \cos(m\theta - n\zeta), \tag{19}$$

$$4\pi e n_s(NU \rightarrow NU) = -k_D^2 [1 + \zeta_{m,n} Z_p(\zeta_{m,n})] \tilde{\phi}_s \times \sin(m\theta - n\zeta), \tag{20}$$

where $Z_p(\zeta_{m,n})$ is the ordinary plasma dispersion function, which is defined by

$$Z_p(\zeta) = \pi^{-1/2} \int_{-\infty}^{+\infty} dx \frac{1}{x - \zeta} \exp(-x^2). \tag{21}$$

The nonuniform density perturbation caused by the uniform field is obtained by integrating Eq. (15) over velocity space:

$$4\pi e n_s(U \rightarrow NU) = k_D^2 v_\perp \left(\frac{v_T}{\omega_{c,0}} k_\psi \right) \frac{1}{k_{\parallel,m,n} v_T} \alpha_{m,n} Z_2(\zeta) \tilde{\phi}_0 \times \sin(m\theta - n\zeta),$$

$$4\pi e n_c(U \rightarrow NU) = 0. \tag{22}$$

Here,

$$Z_2(\zeta) = \pi^{-1/2} \int dx \frac{\left(x^2 + \frac{1}{2}\right)}{x - \zeta} \exp(-x^2). \tag{23}$$

Summing up the electric charges from electrons and ions induced by the uniform and nonuniform fields and imposing charge neutrality, we obtain

$$\sum_{i,e} 4\pi e n_s(NU \to NU) + \sum_{i,e} 4\pi e n_s(U \to NU)$$
$$= \left(-\{k_{D,e}^2 + k_{D,i}^2[1 + \zeta_{m,n,i} Z_p(\zeta_{m,n,i})]\} \tilde{\phi}_s \right.$$
$$\left. + k_{D,i}^2 \frac{1}{k_{\|,m,n} v_{T,i}} \alpha_{m,n}(k_\psi) Z_2(\zeta_{m,n,i}) \phi_0 \right)$$
$$\times \sin(m\theta - n\zeta) = 0. \tag{24}$$

Here, the subscript (i,e) has been introduced to designate the contributing species; so far the expressions have been applicable both to electrons and ions. The adiabatic approximation, $k_{D,e}^2[1+\zeta_{m,n,e} Z_p(\zeta_{m,n,e})] \to k_{D,e}^2$, has been made in the calculation of the electron density perturbation due to the nonuniform field. Similarly, only the ion contribution is taken into consideration in calculating the density perturbation due to the uniform field; $Z_2(\zeta_{m,n,e})$ is small due to the small value of $\zeta_{m,n,e}$. From Eq. (24), we obtain

$$\tilde{\phi}_s = v_{T,i} \left(k_\psi \frac{v_T}{\omega_{c,0}} \right) \frac{1}{k_{\|,m,n} v_{T,i}} \alpha_{m,n} \chi_{m,n} Z_2(\zeta_{m,n,i}) \tilde{\phi}_0. \tag{25}$$

Here, we have defined

$$\chi(\zeta_{m,n,i}) = \{k_{D,e}^2/k_{D,i}^2 + [1 + \zeta_{m,n,i} Z_p(\zeta_{m,n,i})]^{-1}\} Z_2(\zeta_{m,n,i}) \tag{26}$$

for uses in the discussions in the following sections. In similar calculations using $\Sigma_{i,e} 4\pi e[\tilde{n}_c(U \to NU) + \tilde{n}_c(U \to NU)] = 0$, we obtain simultaneously $\tilde{\phi}_c = 0$. It is noted that the only electron-related parameter in Eq. (26) is $T_e/T_i \propto (k_{D,e}^2/k_{D,i}^2)$ and all other quantities are those of ions.

C. Dispersion relation of the GAM

The radial current across the flux surface due to the uniform field, $J(U)$, is obtained by integrating $e\vec{v}_D \cdot \nabla\psi \tilde{f}_s(U \to NU)$ over the flux surface:

$$J(U) = 4\pi \int \vec{j}(U \to) \cdot d\vec{S}$$
$$= 4\pi \int \sqrt{g} d\theta d\zeta \int dv^3 e \vec{v}_D \cdot \nabla\psi \tilde{f}_s(U \to NU). \tag{27}$$

Substituting Eqs. (5)–(7), we obtain

$$J(U) = -\frac{1}{2} k_D^2 v_T^2 \frac{1}{k_\psi} \left(k_\psi \frac{v_T}{\omega_{c,0}} \right)^2 \alpha_{m,n}^2 \tilde{\phi}_0$$
$$\times \int d^3 v \gamma^2 \left(\frac{1}{\omega - (k_{\|,m,n} v_\|)} + \frac{1}{\omega + (k_{\|,m,n} v_\|)} \right)$$
$$\times (f_0/n_0) \int \sin^2(m\theta - n\zeta) \sqrt{g} d\theta d\zeta$$
$$= k_D^2 \frac{1}{k_\psi} v_T^2 \left(k_\psi \frac{v_T}{\omega_{c,0}} \right)^2 \alpha_{m,n}^2 \frac{1}{k_{\|,m,n} v_T} Z_1(\zeta_{m,n}) \tilde{\phi}_0 \frac{1}{2} V'. \tag{28}$$

Here, we have defined $Z_1(\zeta)$ by

$$Z_1(\zeta) = \pi^{-1/2} \int dx \frac{\left((x)^4 + (x)^2 + \frac{1}{2}\right)}{x - \zeta} \exp(-x^2) \tag{29}$$

and made an approximation $\int \sin^2(m\theta - n\zeta) \sqrt{g} d\theta d\zeta \sim \frac{1}{2} V'$ in the last transformation, $\tilde{f}_c(U \to NU)$ makes no contributions after integration over velocity space.

Similarly, the current across the flux surface caused by the nonuniform field is obtained as follows by use of Eq. (17):

$$J(NU) = 4\pi \int \vec{j}(NU \to) \cdot d\vec{S}$$
$$= 4\pi \int \sqrt{g} d\theta d\zeta \int dv^3 e \vec{v}_D \cdot \nabla\psi \tilde{f}_s(NU \to NU)$$
$$= k_D^2 v_T^2 \frac{1}{k_\psi} \left(k_\psi \frac{v_T}{\omega_{c,0}} \right)^2 \alpha_{m,n}^2 \tilde{\phi}_0 \frac{\omega}{k_{\|,m,n} v_T}$$
$$\times \int d^3 v \left(\frac{\gamma}{\omega - (k_{\|,m,n} v_\|)} + \frac{\gamma}{\omega + (k_{\|,m,n} v_\|)} \right)$$
$$\times (f_0/n_0) \int \sin^2(m\theta - n\zeta) \sqrt{g} d\theta d\zeta =$$
$$- k_D^2 v_T \frac{1}{k_\psi} \left(k_\psi \frac{v_T}{\omega_{c,0}} \right) \alpha_{m,n}^2 \zeta_{m,n} Z_2(\zeta_{m,n}) \tilde{\phi}_s \frac{1}{2} V'. \tag{30}$$

Substituting $\tilde{\phi}_s$ given by Eq. (25) into Eq. (30), the sum of the radial currents $J_{\text{geo}} = J(U) + J(NU)$ is given by

$$J_{\text{geo}} = k_D^2 v_T^2 \frac{1}{k_\psi} \left(k_\psi \frac{v_T}{\omega_{c,0}} \right)^2 \alpha_{m,n}^2 \frac{1}{2} V' \frac{1}{k_{\|,m,n} v_T} [Z_1(\zeta_{m,n})$$
$$- \chi_{m,n} \zeta_{m,n} Z_2(\zeta_{m,n})] \tilde{\phi}_0. \tag{31}$$

The subscript geo indicates that the quantity is due to the geodesic curvature. Similarly, "geodesic current" shall mean current that is due to the geodesic curvature, distinguished from the classical polarization current. We use the following formula of classical polarization current:

$$\vec{j}_p = i k_\psi \int \frac{\omega_{p,i}^2}{\omega^2} \frac{\omega}{4\pi i} \frac{d\tilde{\phi}_0}{d\psi} \vec{\nabla}\psi$$
$$= i \frac{1}{2} \frac{k_{D,i}^2}{k_\psi} \int \left(\frac{k_\psi v_{T,i}}{\omega_{c,i}} \right)^2 \frac{\omega}{4\pi i} \frac{d\tilde{\phi}_0}{d\psi} \vec{\nabla}\psi, \tag{32}$$

and integrate it over the flux surface to calculate the total poloidal current J_{pol}.

$$J_{\text{pol}} = 4\pi \int \vec{j}_p \cdot d\vec{S} = \frac{\omega}{4\pi} k_\psi \omega_{p,i}^2 \int \sqrt{g} d\theta d\zeta \frac{1}{\omega^2} |\vec{\nabla}\psi|^2$$
$$= \frac{\omega}{2} k_{D,i}^2 \frac{1}{k_\psi} \left(\frac{k_\psi v_T}{\omega_{c,0}} \right)^2 \frac{1}{q^2} I_\psi^2 B_0^2 V'. \tag{33}$$

One of the geometric factors I_ψ^2 is defined here by

$$\frac{1}{q^2}l_\psi^2 B_0^2 V' \equiv \int \sqrt{g}d\theta d\zeta \frac{\omega_{c,0}^2}{\omega^2}|\vec{\nabla}\psi|^2 \sim \frac{1}{q^2}\int \sqrt{g}d\theta d\zeta |\vec{\nabla}\Phi|^2. \tag{34}$$

It is related to the scale factor of the ψ coordinate. However, it may be approximated (for easy calculations) by the peripheral length of the poloidal cross section of the plasma. Through the discussion above, it was shown that all the mechanisms causing radial currents are proportional to $(k_\psi v_T/\omega_{c,0})^2$, indicating that they are a part of the lowest order finite Larmor radius effect. Therefore, only ion contributions are retained, so that the obvious subscript i is saved; T_e appears as a parameter to represent electrons only in $\chi_{m,n}$.

The dispersion relation is obtained by balancing the classical polarization current with the geodesic currents:

$$\begin{aligned} D &= 4\pi J_{\mathrm{pol}}(U) + 4\pi J(U) + 4\pi J(NU) \\ &= \frac{1}{2}k_D^2 \frac{1}{k_\psi}\left(\frac{k_\psi v_T}{\omega_{c,0}^2}\right)^2 \frac{1}{q^2}l_\psi^2 B_0^2 V' \\ &\quad \times \left(\omega + q^2 \frac{1}{B_0^2 l_\psi^2}\alpha_{m,n}^2 \frac{v_T^2}{(k_{\|,m,n}v_T)}[Z_1(\zeta_{m,n}) \right. \\ &\quad \left. - \chi_{m,n}\zeta_{m,n}Z_2(\zeta_{m,n})]\right)\tilde{\phi}_0 = 0, \end{aligned} \tag{35}$$

or a simplified formula

$$\begin{aligned} D &= i\tilde{\sigma}\cdot\left(\omega + \tilde{\omega}^2 \sum_{m,n} \frac{\tilde{\eta}_{m,n}^2}{(k_{\|,m,n}v_T)}[Z_1(\zeta_{m,n}) \right. \\ &\quad \left. - \chi_{m,n}\zeta_{m,n}Z_2(\zeta_{m,n})]\right)\frac{d\tilde{\phi}_0}{d\psi} = 0 \end{aligned} \tag{36}$$

is obtained by defining the following quantities:

$$\begin{aligned} \tilde{\sigma} &\equiv \frac{1}{2}k_D^2\left(\frac{v_T}{\omega_{c,0}^2}\right)^2 \frac{1}{q^2}l_\psi^2 B_0^2 V', \\ \tilde{\eta}^2 &\equiv (m + nB_\theta/B_\zeta)^2 \frac{\delta^2(\psi)}{(l_\psi/2\pi R_0)^2} \end{aligned} \tag{37}$$

and

$$\tilde{\omega}_G^2 = v_T^2/R_0^2. \tag{38}$$

Here, $\tilde{\sigma}$ is the proportionality constant of the classical polarization current and $\tilde{\omega}_G^2$ is the GAM frequency for a standard tokamak configuration. $\tilde{\eta}_{m,n}^2$ is the other geometric factor characterizing the confining magnetic configuration. This equation correctly reproduces the results of Ref. 32 as to the radial current due to the uniform field, and a modification to the radial current due to the nonuniform field has been made resulting from the improved model used here.

III. APPLICATIONS TO TOKAMAKS

A. Basic dispersion equation for a simple tokamak

The dispersion relations of the GAM for tokamaks are obtained choosing the $n=0$ harmonics selectively; the poloidal mode number m can be retained to incorporate shaping of the plasma cross section, e.g., ellipticity and triangularity. For a tokamak of circular cross section, only the $m=1$ term is retained in good approximation to reduce Eq. (36) to a simpler form:

$$D = i\tilde{\sigma}\cdot(k_\| v_T)\{\zeta + q^2[Z_1(\zeta) - \chi\zeta Z_2(\zeta)]\} = 0, \tag{39}$$

where replacements $k_{\|,m=1,n=0} \to 1/qR_0 \to k_\|$, $\zeta_{m=1,n=0} \to \omega/k_\| v_T \to \zeta$, $l_\psi = 2\pi r$, and $\delta_{m=1,n=0} = \varepsilon = r/R_0$ were made in Eqs. (36) and (37) to obtain the relation

$$\frac{1}{k_\| v_T}\sum_{m,n}\frac{\tilde{\eta}_{m,n}^2}{(k_{\|,m,n}v_T)} \to \frac{\tilde{\eta}_{1,0}^2}{(k_\| v_T)^2}\tilde{\omega}^2 \to q^2. \tag{40}$$

Equation (39) is solved in the following sections for ζ, and ω is calculated by using the relation $\zeta = \omega/k_\| v_T$, i.e., ζ and ω are identified.

We have introduced three kinds of dispersion functions $Z_p(\zeta)$, $Z_2(\zeta)$, and $Z_1(\zeta)$ defined by Eqs. (21), (23), and (29), respectively. It is known that the latter two functions can be rewritten by using $Z_p(\zeta)$ (see the Appendix for their relations and expressions in series and asymptotic expansion). These three functions are different in the multipliers, γ^0, γ^1, and γ^2, in the integrand. They reflect the multiplicity of the intervention of the geodesic curvature in one process. In Fig. 1, they are plotted versus the argument ζ showing different behaviors in the low frequency range.

B. Characteristics of the GAM for two typical parameters: $T_e/T_i=1$ and $T_e/T_i>1$

The formulation in the previous section states that the geodesic current J_{geo} consists of two parts: the part caused by the uniform field, $J(U)=q^2Z_1(\zeta)$, and the other part caused by the nonuniform field, $J(NU)=-q^2\chi\zeta Z_2(\zeta)$. Here, the common factor $i\tilde{\sigma}\cdot(k_\| v_T)$ in Eq. (39) has been dropped; in this framework the polarization current is expressed as $J_{\mathrm{pol}}=\zeta$. These two geodesic terms are calculated and shown in Figs. 2(a) and 2(b) assuming $T_e/T_i=1$, manifesting that they are different in the dependences on ζ and are similar in amplitudes. Thus, the uniform and nonuniform fields make similar-sized contributions to the radial current in the standard case of $T_e/T_i=1$.

Figures 3(a) and 3(b) show how the GAM frequencies are determined for the two typical cases of $T_e/T_i=1$ and $T_e/T_i=5$; $q=2$ is assumed common to the two cases. The solid curves give the sum of the geodesic currents $J_{\mathrm{geo}}=J(U)+J(NU)$ and the dotted curves give the imaginary parts. The straight lines give the classical polarization current $J_{\mathrm{pol}}=\zeta$ displayed with its sign reversed: As formulated in the previous section, the GAM frequencies are obtained using the ζ values where the curves and straight lines cross. In Figs. 3(a) and 3(b), GAM frequency $\zeta=\zeta_{\mathrm{GAM}}$ is determined to be 3.5 and 5.5, respectively.

These GAM frequencies are interpreted as the ordinary GAM frequencies obtained readily from the MHD equations and classified in this paper, as the first group of solutions.

The second group of solutions is found in the low frequency range: $\zeta=1.3$ in Fig. 3(a) and $\zeta=2.1$ in Fig. 3(b). They suggest that there are two solutions in the GAM frequency range if there is one solution in the first group. These

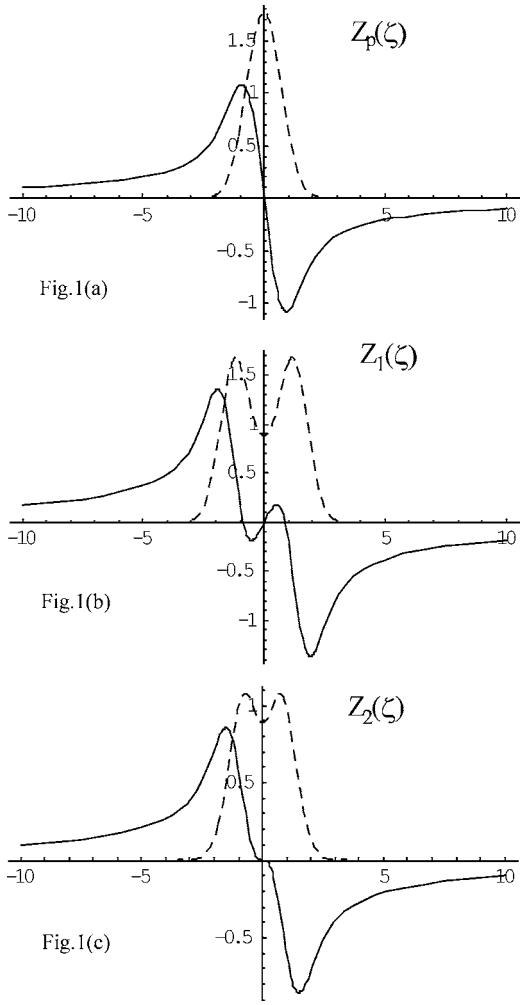

FIG. 1. The dependences of the three dispersion functions on ζ; $Z_1(\zeta)$, $Z_2(\zeta)$, and $Z_p(\zeta)$ are shown in (a), (b), and (c), respectively. Their definitions are given by Eqs. (29), (23), and (21). They show different ζ dependences due to the different weighting functions in their integrals. Particularly, $Z_1(\zeta)$ is unique having a positive slope around $\zeta=0$, which can be regarded as a neoclassical polarization current due to passing particles. $Z_p(\zeta)$ is the well-known plasma dispersion function that appears limitedly in χ [see Eq. (26)], where geodesic curvature does not play a role.

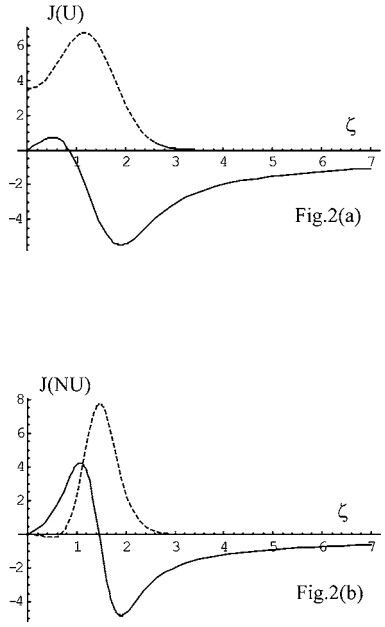

FIG. 2. The radial currents $J(U)$ and $J(NU)$: (a) shows $J(U)=q^2Z_1(\zeta)$, the radial current driven by the uniform potential field and (b) shows $J(NU)=-q^2[\chi Z_2(\zeta)]Z_2(\zeta)$, the current driven by the nonuniform potential field. Calculations were made with parameters $T_e/T_i=1$ and q=2. $J(U)$ has the same form as $Z_1(\zeta)$ shown in Fig. 1(a). $J(NU)$ has a quite different dependence on ζ from that of $Z_2(\zeta)$ due to the presence of the shielding factor, and its size strongly depends on the value of T_e/T_i.

solutions of the second group may join the candidates for one of the two frequencies of GAM-like oscillations reported in JIPP-T-IIU[19] and ASDEX U[25] experimental results. It is noted that there is always a solution around $\zeta\sim 0$, which may be identified as a stationary zonal flow and classified in this paper as the third group of solutions.

To conclude this section, there are two GAM-like frequencies in addition to the stationary zonal flow for both cases of $T_e/T_i=1$ and $T_e/T_i=5$.

C. Interpretation of the calculation results

1. Ordinary GAM

Equation (39) is transformed as

$$[\zeta+q^2Z_1(\zeta)]\{\tau_e^{-1}+[1+\zeta\cdot Z_p(\zeta)]\}=q^2\chi\zeta Z_2(\zeta), \tag{41}$$

where we have introduced for simplification a parameter $\tau_e\equiv k_{D,i}^2/k_{D,e}^2=Z_i(T_e/T_i)$. If the term on the right-hand side $q^2\chi\zeta Z_2(\zeta)$ is small, Eq. (41) gives the two decoupled dispersion relations

$$[\zeta+q^2Z_1(\zeta)]=0 \tag{42}$$

and

$$\{\tau_e^{-1}+[1+\zeta\cdot Z_p(\zeta)]\}=0. \tag{43}$$

Therefore, Eq. (41) is viewed as an equation for predicting the coupling of the two modes with $q^2\chi\zeta Z_2(\zeta)$ regarded as a coupling constant. Equation (42) gives the standard kinetic GAM frequency treated in Ref. 29, and Eq. (43), which is the dispersion equation of electrostatic waves, has two solutions in the case of $\tau_e>1$. The interpretation of results obtained in Sec. III B is simple as to the first group of solutions; we expand asymptotically the three terms composing Eq. (41) to obtain a dispersion relation

$$\left[\zeta^2-q^2\left(\frac{7}{4}+\tau_e\right)\right]\left(\zeta^2-\frac{1}{2}\tau_e\right)=\left(\frac{23}{8}q^2+\frac{3}{4}\tau_e+2(q^2\tau_e)+\frac{\tau_e}{2}q^2\right). \tag{44}$$

The following solution results from this equation:

$$\zeta_{\mathrm{GAM}}^2=\left(\frac{7}{4}q^2+q^2\tau_e\right)+\frac{1}{(\zeta_{\mathrm{GAM},0}^2-\tau_e/2)}\left[\frac{23}{8}q^2+\frac{3}{4}\tau_e+2(q^2\tau_e)-\frac{7}{8}q^2\tau_e\right], \tag{45}$$

where

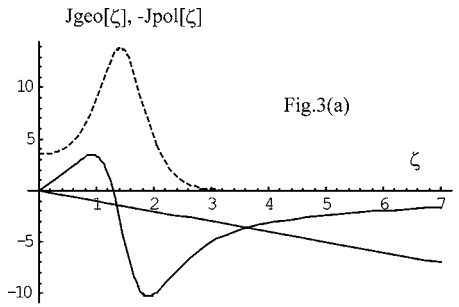

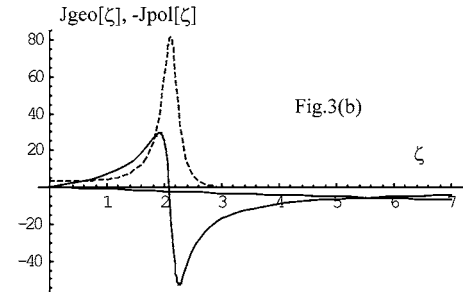

FIG. 3. Determination of the GAM frequency: (a) $T_e/T_i=1$; (b) $T_e/T_i=5$. The real and imaginary parts of geodesic current $J_{\text{geo}}=J(U)+J(NU)$ are shown by solid and broken curves. Polarization currents are shown in (a) and (b) by straight lines with their sign reversed. The GAM frequencies are determined as the ζ values where J_{pol} equals $J_{\text{geo}}=J(U)+J(NU)$. Comparing (a) and (b), it is found that the geodesic current is enhanced in the case of $T_e>T_i$.

$$\zeta^2_{\text{GAM},0}=\left[q^2\left(\frac{7}{4}+\tau_e\right)\right]. \tag{46}$$

This is a kinetic elaboration GAM frequency over the MHD description and fits in the form of Eq. (1) with $\omega_{\text{GAM},0}=\sqrt{2[T_e+(7/4)T_i]/m_i}/R$ in place of $\omega_{\text{MHD},0}=\sqrt{2[T_e+(5/3)T_i]/m_i}/R$ and several of the correction terms having forms of $\delta\omega^2\propto k_\parallel^2(T_i/m_i)$ and $\propto k_\parallel^2(T_e/m_i)$. $\zeta^2_{\text{GAM},0}$ accounts for the numerical result in Sec. III B that the GAM frequency is higher if T_e/T_i is larger. It is noted that the correction terms contain various parallel dynamics of the particles, though they play a minor role in the first group of solutions (ordinary GAM) if q is sufficiently large.

2. GAM-like solutions in a lower frequency range

The second group of solutions emerges due to the swing of the geodesic currents, $J(U)$ and $J(NU)$, in the lower frequency range: In order to study the mechanism of these solutions (the GAM-like mode in the lower frequency range), we need to study the properties of $J(U)$ and $J(NU)$ in more detail and consider their relative importance. We have introduced $\chi=N_u/D_e$ in Sec. II B with denominator $D_e\equiv\{k^2_{D,e}/k^2_{D,i}+[1+\zeta Z_p(\zeta)]\}$ and numerator $N_u=Z_2(\zeta)$; χ is interpreted as the response function of the nonuniform field $\tilde{\phi}_s$ to the uniform field $\tilde{\phi}_0$. N_u is proportional to the charge

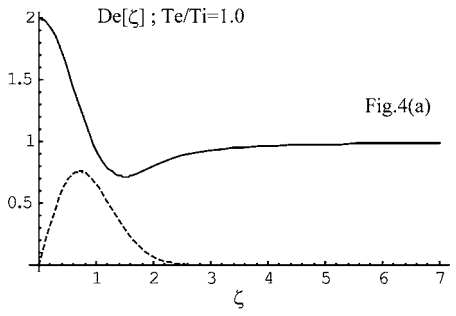

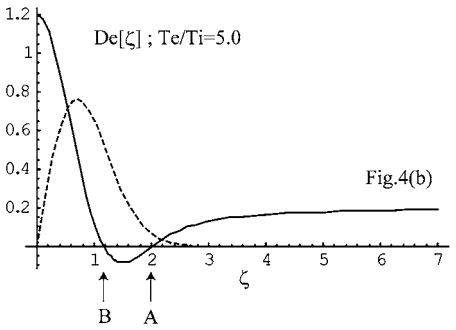

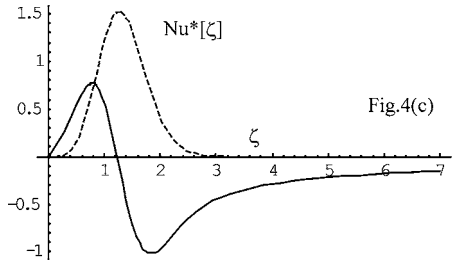

FIG. 4. The components determining $J(NU)=-q^2N_u^*/D_e$. The denominator D_e and numerator N_u^* are shown vs ζ. (a) shows the D_e calculated with $T_e/T_i=1$ and (b) with $T_e/T_i=5$. A critical difference is found between the two cases: In the case of $T_e/T_i=1$ the D_e shows a moderate variation from 2 to 1 as ζ varies from 0 to 7. In the case of $T_e/T_i=5$, D_e crosses the abscissa twice as ζ varies from 0 to 7 [see the indication in (b) made by the arrows with labels A and B]. Physically, this effect is attributed to the coupling of the GAM with two kinds of sound waves. (c) shows the numerator N_u^*, which is common to the two cases, being independent of the value of T_e/T_i.

directly induced by the external uniform field $\tilde{\phi}_0$ and D_e is the shielding factor normalized by $k^2_{D,i}$. It is noted that χ takes a large value for the ζ, satisfying

$$D_e\equiv\{k^2_{D,e}/k^2_{D,i}+[1+\zeta Z_p(\zeta)]\}=0. \tag{47}$$

Then, χ is regarded as an enhancement factor rather than just a shielding factor. To study the total effects of a nonuniform field on geodesic current, we define $\chi^*=N_u^*/D_e$ with $N_u^*=\zeta Z_2\cdot Z_2$ so that

$$J(NU)=-q^2\chi^*. \tag{48}$$

In Fig. 4(a), the real and imaginary parts of D_e, $\text{Re}[D_e]$ and $\text{Im}[D_e]$, are plotted versus ζ in the case of $\tau_e=1$. The real part (reactive part) varies from $2(\approx 1+1/\tau_e)$ to $1(\approx 1/\tau_e)$ as ζ varies from 0 to 7 ($\sim$ infinity) corresponding to the variation of $\zeta Z_p(\zeta)$ from 0 to -1. This variation indicates that Debye screening of ions vanishes at a large value of ζ while that of electron persists. In general, D_e^{-1} does not show pe-

culiar variations but shows monotonous variations for the case of $\tau_e=1$. The swing of $J(NU)$ in Fig. 3(a) is attributed to the sign change of the numerator $N_u^*=\zeta Z_2\cdot Z_2$ as shown in Fig. 4(c); a phase variation in $Z_2(\zeta)$ by $\pi/2$ causes that of N_u^* by π.

In the case of $\tau_e=5$, the situation is quite different: In Fig. 4(b), Re$[D_e]$ and Im$[D_e]$ are plotted versus ζ. Re$[D_e]$ descends from $1.2=(1+1/\tau_e)$ for the variation of ζ from 0 to 7 and crosses the abscissa twice as indicated by arrows in Fig. 4(b): once at around $\zeta\sim 2.0$ (labeled A) and once at $\zeta\sim 1.2$ (labeled B). The former coincides with the value of $\zeta\sim 2.1$ in Fig. 3(b), where the geodesic current makes a big swing and crosses the abscissa. The meanings of these ζ values are understood by expanding Re$[D_e]$ asymptotically and in series using the expression given in the Appendix.

We obtain the following two forms suitable respectively for the larger and smaller solutions of Re$[D_e]=0$:

$$\mathrm{Re}[D_e]=\frac{1}{\tau_e}\left(1-\frac{1}{2}\tau_e\zeta_l^{-2}-\tau_e\frac{3}{4}\zeta_l^{-4}\right)=0 \tag{49}$$

and

$$\mathrm{Re}[D_e]=\frac{1}{\tau_e}(1+\tau_e-2\tau_e\zeta_s^2)=0. \tag{50}$$

The solutions to Eqs. (49) and (50) for $\tau_e=5$ are $\zeta=1.89$ and $\zeta=0.77$, well approximating the corresponding values $\zeta\sim 2.0$ and $\zeta\sim 1.0$ obtained in Fig. 4(b). [The slight disagreements between them are attributed to inaccuracies of the approximations, Eqs. (49) and (50).] Since the larger and smaller solutions have asymptotic forms $\omega=k_\parallel\sqrt{Z_iT_e/m_i}$ and $\omega=k_\parallel\sqrt{2T_i/m_i}$ for large τ_e, we shall refer to these solutions in this paper as the electron and the ion branch of sound waves, respectively. The electron branch is known as the ion acoustic wave, having weak damping if $\tau_e>1$. The ion branch is less popular and categorized as a class of quasimode having heavier damping. They are inclusively referred to as sound waves. The inversion of $J(NU)$ occurs in the case of $\tau_e>1$ at the ion acoustic wave frequency. Though this inversion of the sign occurs also at the sound wave frequency of ion branch, $J(NU)$ does not change sign there in the case of $\tau_e>1$, because it coincides with that where numerator $\zeta Z_2\cdot Z_2$ changes sign.

The radial current due to the uniform field $J(U)$ also changes sign in the low frequency range. This is attributed to the uniqueness of the $Z_1(\zeta)$, where faster and slower groups of particles carry radial currents in opposite directions. The inversion of the direction occurs due to the population change of ions belonging to the two groups in the lower frequency range.

To summarize this subsection, the geodesic radial currents, $J(U)$ and $J(NU)$, eventually have similar frequency dependences, having currents in the sense of polarization current in the lower frequency range; this is a quite interesting feature that MHD equations cannot describe. The GAM-like mode in the low frequency range is thus attributed to this uniqueness of kinetic responses.

It is also pointed out that the coupling to the branches of sound waves occurs under the condition of $\tau_e>3$. It is supposed that the experimentally observed GAM oscillations under the condition of $T_e/T_i>1$ may contain modes influenced by the ion acoustic mode.

3. Nonuniformity of the potential field

The presence of this effect may be checked in the experiments or in the results of computer simulations by diagnosing the up-down asymmetry of the potential. From the discussion in the previous section we obtain

$$\begin{aligned}\tilde{\phi}_s/\tilde{\phi}_0&=\upsilon_T\left(k_\psi\frac{\upsilon_T}{\omega_{c,0}}\right)\frac{1}{k_{\parallel,m,n}\upsilon_T}\alpha_{m,n}\chi_{m,n}\\&\sim 2\pi\left(k_\psi\frac{\upsilon_T}{\omega_{c,0}}\right)\frac{m}{q}B_0^2|mB^\theta-nB^\zeta|^{-1}\delta_{m,n}\chi_{m,n}.\end{aligned} \tag{51}$$

For tokamaks of a circular plasma cross section, we assume $(m,n)=(1,0)$ and make a substitution $k_\psi\sim k_r(dr/d\psi)\sim k_r(1/2\pi RB_p)$. For a simple tokamak case, we obtain by dropping out subscripts $(m,n)=(1,0)$

$$\tilde{\phi}_s/\tilde{\phi}_0\sim\left(k_r\frac{\upsilon_T}{\omega_{c,0}}\right)\frac{B_0}{B_p}\left(\frac{r}{R_0}\right)\chi\sim-\left(k_r\frac{\upsilon_T}{\omega_{c,0}}\right)\frac{B_0}{B_p}\left(\frac{r}{R_0}\right)\frac{1}{\zeta}, \tag{52}$$

where an approximation $\chi=(Z_iT_e/T_i)Z_2=-(Z_iT_e/T_i)(1/\zeta)$ has been made, which is derived from Eq. (A7) for a large value of ζ.

According to recent experimental observations that $(k_r\upsilon_T/\omega_{c,0})\sim 1/q$, $\tilde{\phi}_s/\tilde{\phi}_0$ may be of the order of $1/\zeta$. Though the latter is regarded as a parameter indicating smallness, $\tilde{\phi}_s/\tilde{\phi}_0$ may be detectable in experiments. If the observed GAM is affected by the ion acoustic mode, the nonuniformity is even enhanced due to the increased χ, making it easier to detect in experiments.

We obtain, for the case of $T_e/T_i=1$, the window in which the GAM can exist as follows:

$$0.83<q. \tag{53}$$

It is expected that GAM may exist in a more limited parameter range than Eq. (53), if the damping is taken into account, and may be practically prevented from existing in the core region of the plasma. On consideration of the possible enhancement of polarization current due to neoclassical effects,[33] the window of the GAM existence may be even narrower. Even under such conditions, the presence of the coupling of GAMs to ion acoustic waves $(T_e/T_i\gg 1)$ may enhance the geodesic current $J(NU)$ and allow the presence of the GAM.

IV. APPLICATION TO HELICAL SYSTEMS

A. Applications to straight helical systems

We first consider a straight helical device with dominant mode numbers $(m,n)=(M,N)$, which is determined by the helical pitch numbers of the device. This gives a good reference for the understanding of the GAM in toroidal helical systems.

By using these integral numbers, the dispersion relation may be written as

$$D = i\tilde{\sigma}\left(\omega + \tilde{\tilde{\omega}}_G^2 \frac{\tilde{\tilde{\eta}}_{M,N}^2}{(k_{\parallel,M,N} v_T)} [Z_1(\zeta_{M,N}) - \chi_{M,N}\zeta_{M,N} Z_2(\zeta_{M,N})] \right). \tag{54}$$

Since single helicity is assumed, the structure of the equation is the same as that of tokamaks. The variable $\zeta = \omega / v_T k_{\parallel,1,0}$ used in the previous section is simply replaced by $\zeta_{M,N} = \omega / v_T k_{\parallel,M,N}$.

Though the formulation has the same structure, the wave numbers are quite different. While $k_{\parallel,1,0} = B^\theta / B$ in tokamaks, $k_{\parallel,M,N} \equiv (MB^\theta - NB^\zeta)/B \sim -NB^\zeta / B$ in helical systems.

For standard linear helical systems, which have large toroidal pitch numbers, the latter wave number takes on much larger values tan in tokamaks. Physically, it means that the connection length is shorter in helical systems than in tokamaks. This gives the GAM in helical systems different features from those of tokamaks. Since the pressure asymmetry is more easily canceled along the magnetic lines of force, the geodesic radial current has more difficulty balancing the polarization current.

The condition of the GAM existence is obtained analytically for the case of $T_i / T_e = 1$ as

$$0.7 < \left(\tilde{\tilde{\omega}}_G^2 \frac{\tilde{\tilde{\eta}}_{N,M}^2}{(k_{\parallel,N,M} v_T)^2} \right). \tag{55}$$

Substituting $\delta_{N,M}^2 / (l_\psi / 2\pi R_0)^2 \sim 1$, $(MB_\zeta + NB_\theta) \sim MB_\zeta$, and $k_{\parallel,M,N} \sim -N/R_0$, Eq. (53) is approximated by

$$0.83 < \frac{\delta_{M,N}}{(l_\psi / 2\pi R_0)} (M/N). \tag{56}$$

Since M/N is usually small in standard helical systems, the parameter range of GAM existences will be narrower than that of tokamaks. The previous work, Ref. 32, is based on an asymptotic expansion and therefore caution must be taken in applications to the standard parameter $(T_e / T_i = 1)$. An exception is the radial domain where $MB^\theta / NB^\zeta - 1 \approx 0$, in which the connection length becomes larger and this boundary of GAM existence is relaxed.

Figures 5(a) and 5(b) show the determination of GAM frequencies in a straight helical system: $T_e / T_i = 1$ and $T_e / T_i = 5$. The geodesic current J_{geo} and the polarization currents J_{pol} are plotted versus ζ (in place of $\zeta_{M,N}$) to facilitate a smooth connection to the next subsection. Shortage of J_{geo} relative to J_{pol} is evident in Fig. 5(a), where $T_e / T_i = 1$ is assumed. Figure 5(b) shows that a helical-type GAM can exist in the cases of $T_e / T_i > 1$. This is partly due to the general enhancement of the geodesic current, but more importantly, due to the coupling with ion acoustic mode.

Returning to Eqs. (47) and (49), we may write

$$D_e = \{\tau_e^{-1} + [1 + \zeta Z_p(\zeta)]\} \approx \left[\tau_e^{-1} - \left(\frac{1}{2}\frac{1}{\zeta^2} + \frac{3}{4}\frac{1}{\zeta^4} \right) \right]$$

$$\approx \frac{2}{\zeta_0} \tau_e^{-1} [(\zeta - \zeta_0) + i\zeta_0^2 \tau_e \delta / 2]. \tag{57}$$

Here, $\zeta_0^2 = \frac{1}{2}\tau_e + 3$ is the frequency of the ion acoustic wave and $\delta = \text{Im}[Z_p(\zeta_0)]$ is the imaginary part of $Z_p(\zeta)$ calculated at $\zeta = \zeta_0$.

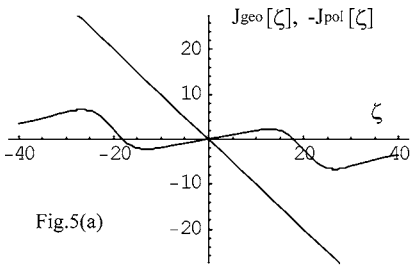

Fig.5(a)

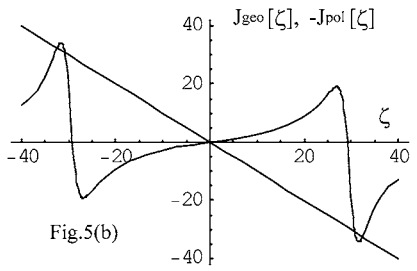

Fig.5(b)

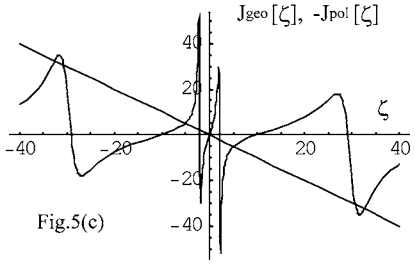

Fig.5(c)

FIG. 5. Determination of the GAM frequency in helical systems. Real parts of $J_{\text{geo}}[\zeta]$ and $-J_{\text{pol}}[\zeta]$ are plotted vs ζ for three cases: (a) and (b) show the calculation in the cases of a straight helical system; $T_e / T_i = 1$ is assumed in (a) and $T_e / T_i = 5$ in (b). In the latter case with high T_e / T_i, geodesic current is enhanced and two solutions emerge in the helical GAM frequency range. (c) is the calculation for a mixed helicity case; the two modes in the different frequency ranges are nearly independent and they affect each other perturbatively.

Equation (41) is then approximated as follows in the vicinity of $\zeta = \zeta_0$:

$$\text{Re}\left(\frac{1}{[(\zeta - \zeta_0) + i(\tau_e \zeta_0^2 \delta / 2)]} \right) = b = \frac{2a}{\zeta_0} \tau_e^{-1}. \tag{58}$$

Here, $a \equiv \text{Re}\{[\zeta_0 + q^2 Z_1(\zeta_0)] / q^2 \zeta [Z_2(\zeta_0)]^2\}$ and is regarded to be positive and small in the cases of inferiority of the geodesic currents to the polarization current.

We obtain a quadratic equation

$$(\zeta - \zeta_0)^2 - \frac{\zeta_0}{2a} \tau_e (\zeta - \zeta_0) + (\tau_e \zeta_0^2 \delta / 2)^2 = 0 \tag{59}$$

to which the following two solutions follow:

$$(\zeta - \zeta_0) = \frac{1}{2} \left[\left(\frac{\zeta_0}{2a} \tau_e \right) \pm \sqrt{\left(\frac{\zeta_0}{2a} \tau_e \right)^2 - (\tau_e \zeta_0^2 \delta)^2} \right]. \tag{60}$$

Since the right-hand side is positive independent of the sign, two solutions are predicted to be above the ion acoustic wave frequency: one above ζ_0 by $\delta\zeta \sim \tau_e \zeta_0 / 2a$ and the other

by $\delta\zeta \sim \tau_e a \zeta_0^3 \delta^2/2$. The former solution (+) is interpreted as a continuous modification from the ordinary GAM in tokamaks. The latter (−) is conjectured to have heavier damping. With the present assumptions, $a>1$ and $\delta \ll 1$, neither of the two solutions is far from ζ_0.

Coupling of GAM with the ion acoustic mode in helical system has more significant effects than in tokamaks: It not only causes the frequency shift of GAM but also enhances the geodesic current to allow its existence. As is shown in Eq. (51), such GAM will have a larger fraction of nonuniform field $\phi_s/\tilde{\phi}_0 \propto \sin(M\theta - N\zeta)$ than that in the tokamaks $\phi_s/\tilde{\phi}_0 \propto \sin\theta$.

B. Applications to toroidal helical systems

Practical helical systems are toroidal and intrinsically have toroidal curvature. Therefore it is necessary to consider at least two kinds of curvatures: For the CHS device $(m,n)=(M,N)=(2,8)$ and $(m,n)=(1,0)$. The sizes of the tokamak and helical ripples are similar in size $\delta_{M,N}^2 \approx \delta_{1,0}^2$ at around the $r/a \sim 2/3$, where r is the averaged minor radius and a is that of the outermost closed flux surface. As estimated in the previous examples, the curvature due to the toroidal ripple plays a more important role due to the longer connection length. From this point of view, toroidal helical systems are expected to have at least tokamak-type GAMs even in the standard range of plasma parameters, $T_e/T_i \sim 1$. They appear in the similar frequency range of tokamak GAM and are classified as a tokomak-type GAMs in toroidal helical systems.

With the coupling of GAM with the ion acoustic mode, helical ripples may play a substantial role. We start with the following model equation:

$$D = i\tilde{\sigma}\cdot\left(\omega + \tilde{\tilde{\omega}}_G^2 \frac{\tilde{\eta}_{1,0}^2}{(k_{\parallel,1,0}v_T)}[Z_1(\zeta_{1,0}) + \chi_{1,0}\zeta_{1,0}Z_2(\zeta_{1,0})] + \tilde{\tilde{\omega}}_G^2 \frac{\tilde{\eta}_{M,N}^2}{(k_{\parallel,M,N}v_T)}[Z_1(\zeta_{M,N}) + \chi_{M,N}\zeta_{M,N}Z_2(\zeta_{M,N})]\right). \tag{61}$$

Figure 5(c) shows the calculations to determine the GAM frequency in the case of $T_e/T_i=5$, where $\zeta=\zeta_{m=1,n=0} \sim qN\zeta_{M,N}$ is taken on the abscissa and radial currents on the ordinate. The solid curve shows the sum of the geodesic currents due to the tokamak curvature $(m,n)=(1,0)$ and helical curvature $(m,n)=(M=2,N=8)$. The straight line shows the classical polarization current with a reversed sign. $\tilde{\eta}_{M,N}=3$ is assumed to specify the strength of the helical ripple relative to the tokamak ripple, which is a value representing one third minor radius.

In Fig. 5(c), a pair of solutions is found around $\zeta=\zeta_{m=1,n=0}=5.5$, where the toroidal $(m,n)=(1,0)$ magnetic ripple plays a dominant role. The GAM will then have the features of the tokamak type. Another pair of solutions is found around $\zeta=\zeta_{m=1,n=0}=32$ in Fig. 5(c), where the radial current due to $(m,n)=(M=2,N=8)$ magnetic ripple plays a dominant role. The GAM will thus have features of helical GAM. It is noted that this helical-type GAM is also dependent on $\tilde{\eta}_{M,N}$, the parameter representing the intensity of the helical geodesic curvatures relative to that of a tokamak. Thus it is predicted that a helical-type GAM emerges as the helical ripple is increased. Such a change of the mode structure may occur in heliotron-type devices spatially, because it is known that the relative intensity of the helical ripples increases with the minor radius.

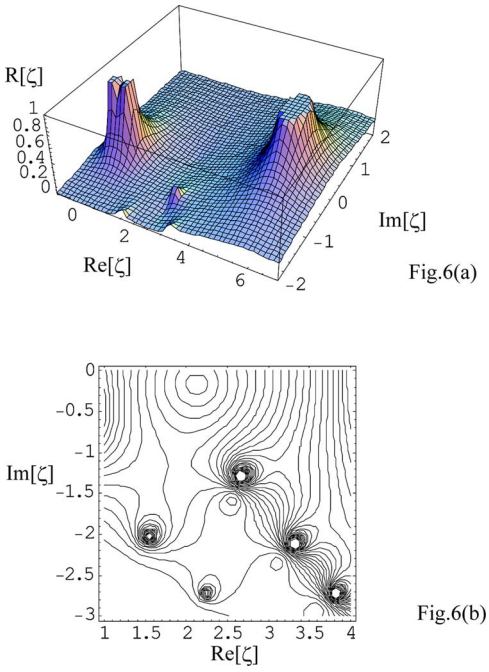

Fig.6(a)

Fig.6(b)

FIG. 6. Full complex calculation of the response function for a simple tokamak case: Total response function $|R(\zeta)|$ is calculated over complex $\zeta(=\zeta_{m=1,n=0} \sim qN\zeta_{M,N})$ plane for $(T_e/T_i=5$ and $q=2.0)$: The solutions of GAM are given as poles of the response function. In Fig. 5(a), two poles are found in the fourth quadrant of the ω plane. The one at $\mathrm{Re}[\zeta] \sim 5.5$ is the ordinary GAM; this mode is well defined having $\mathrm{Im}[\zeta] \sim 0.0$. (b) gives the magnified view of (a), where five satellite poles are found.

V. FULL COMPLEX ANALYSES

A. Simple tokamak case

Full complex analyses are required for more exact examinations of the dispersion relation. In order to do this, we formally recover an external driving term $4\pi J_{\mathrm{ext}}(\omega)$ on the right-hand side of Eq. (36) and write

$$\frac{d\tilde{\phi}_0(\omega)}{d\psi} = \frac{4\pi J_{\mathrm{ext}}[\omega]}{D[\zeta(\omega)]} \equiv R(\omega)J_{\mathrm{ext}}(\omega). \tag{62}$$

Here, $R(\omega) \propto D(\omega)^{-1}$ is regarded as the response function of the electric field $d\tilde{\phi}_0(\omega)/d\psi$ to the external current $J_{\mathrm{ext}}(\omega)$, which is assumed to be caused by turbulence through nonlinear phenomena including Reynolds stress and Stringer mechanisms. ω and ζ are identified due to the relation $\zeta=\omega/k_\parallel v_T$. In Secs. III and IV, we derived the dispersion relation assuming $\mathrm{Re}[D]=0$; if ζ is real it is equivalent to $D^H=0$ with D^H the Hermitian part of D.

Figure 6(a) shows the calculation made in a tokamak case: the response function $|R[\zeta]|$ is shown in a three-dimensional (3D) plot over $\zeta_r=\mathrm{Re}[\zeta]$ and $\zeta_i=\mathrm{Im}[\zeta]$. Here, parameters $q=2$ and $\tau_e=5$ are used.

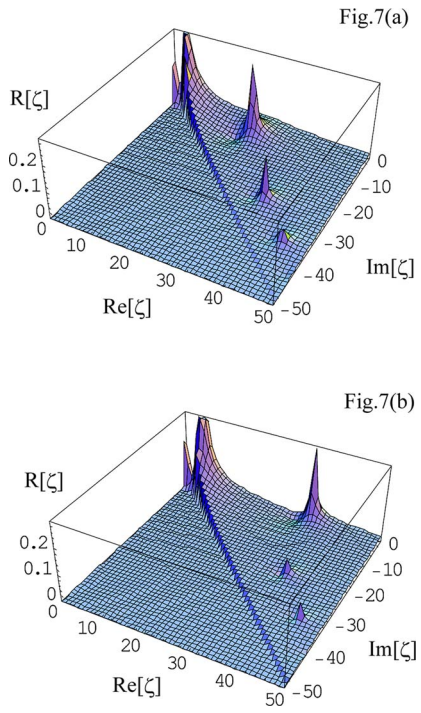

FIG. 7. Full complex calculation of the response function in a helical system (mixed-helicity case): Total response function $|R(\zeta)|$ is calculated over complex ζ plane; parameter sets ($T_e/T_i=1$, $\tilde{\eta}_{M,N}=3$, $N=8$) and ($T_e/T_i=5$, $\tilde{\eta}_{M,N}=3$, $N=8$) were used in calculating (a) and (b), respectively. Two major peaks appear in each figure corresponding to tokamak and helical ripples. In (b), where T_e/T_i is larger, the geodesic current is magnified and a helical-type GAM solution appears with a smaller Im[ζ] value.

In this display, the presence of peaks suggest the possible presence of poles of $R(\omega)$, i.e., the frequency of the GAM can be determined. There are two outstanding peaks found in the fourth quadrant of the ω plane: the one at around ($\zeta_r=5.5$, $\zeta_i=0.0$) corresponds to the ordinary GAM, having a similar value of ζ_r that was obtained from Fig. 3(b). The other one at around ($\zeta_r=0.0$, $\zeta_i=0.0$) corresponds to the stationary zonal flow. Within the framework of collisionless damping (plateau regime), the stationary zonal flow has a finite damping rate. Figure 6(a) also has small peaks, suggesting the presence of another group of poles. Figure 6(b) is an expanded view of Fig. 6(a) in the form of a contour plot; each of the peaks is confirmed to be a pole by using Cauchy's theorem. Thus it is found that the GAM-like mode in the lower frequency range, which we discussed in Sec. III, is transformed into modes with substantial damping rate in the full complex analysis.

B. Mixed helicity case

GAM in mixed helicity configurations has been studied using the same full complex analyses as described in Sec.V A. Figures 7(a) and 7(b) give global views of the absolute value of the response function $|R[\zeta]|$, shown in a 3D plot over Re[ζ] and Im[ζ]. The parameters used in the calculations are commonly $q=2$, $(N,M)=(2,8)$, and $\tilde{\eta}_{M,N}=3$, and the parameter T_e/T_i is different between the two cases: Equation (61) shows that P is a function of ω via the dependences on $\zeta_{m=1,n=0}(\omega)$ and $\zeta_{M,N}(\omega)$ distinguishing if the cause of their contributions is due to tokamak ripple or helical ripple.

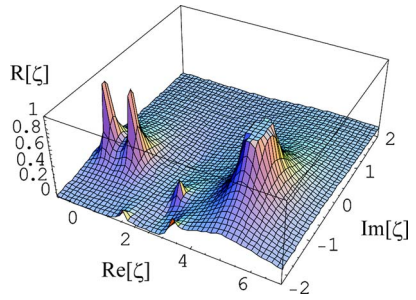

FIG. 8. The magnified view of Fig. 7(a): The low frequency range of Fig. 7(a) is shown elucidating a tokamak-type GAM in the mixed helicity system: Since the parameter set used ($q=2$, $T_e/T_i=5$, $\tilde{\eta}_{M,N}=3$, $N=8$) is the same as that used in Fig. 6(a), a useful comparison can be made: The GAM pole shifts deeper in the complex plane due to the mixed helicity and the pole of stationary zonal flow gains a real frequency.

Since they are mutually related by

$$\zeta_{m=1,n=0} = (M - qN)\zeta_{M,N}, \tag{63}$$

$\zeta_{m=1,n=0}$ is chosen as a single variable ζ. $|R[\zeta]|$ is then 3D displayed over Re[ζ] and Im[ζ].

In Fig. 7(a), where we assume $T_e/T_i=1$, the helical-type GAM is found at $(\zeta_r,\zeta_i)=(25.0,-8.0)$. It is noted that a solution is given in the full complex analysis under the condition of $T_e/T_i=1$, where no solution was found in Sec. IV [see Fig. 5(a)]; the solution has instead a significantly larger damping rate. We can also recognize two satellite poles, which, however, may be more difficult to find in experiments because they are deeper in the lower half ζ plane.

In Fig. 7(b), where we assume $T_e/T_i=5.0$, the helical-type GAM is found at frequency $(\zeta_r,\zeta_i)=(32.0,\sim 0.0)$. The real frequency is approximately the same as the one we found in Fig. 5(c), and since $\zeta_i \approx 0$, the GAM is predicted to be well defined. We can also recognize two satellite poles like the ones we find in Fig. 6(a), which also may be difficult to find in experiments having a large imaginary part. From the comparison of Figs. 7(a) and 7(b), it is found that the GAM frequency is higher and the damping rate is lower with increasing T_e.

In the lower frequency range, there are tokamak-type GAMs in both Figs. 7(a) and 7(b). Since this frequency range is crowded, an expanded view of Fig. 7(b) is shown in Fig. 8, facilitating a direct comparison with Fig. 6(a) with the same τ_e assumed. It is found that both of the two major poles corresponding to a tokamak-type GAM and stationary zonal flow have moved deeper into the lower half plane. The only difference in Fig. 8 from Fig. 6(a) is the presence of an added helical ripple in the former. In the low frequency range the tokamak ripple plays a dominant role and no significant difference is found in the real frequency. A significant difference between the two cases is however found in Im[ω], which is attributed to the additional damping mechanism due to the helical ripple, which can be treated perturbatively as has been shown in Refs. 32, 35, and 36.

VI. DISCUSSIONS

The possible presence of GAM in the lower frequency was suggested in this paper by using the drift kinetic equation. This mode, however, turned out to have a significant damping rate in a full complex analysis, and therefore it is difficult to convincingly predict that it will be observed in experiments. However, it may be noted that these predictions are results of solving the drift kinetic equation in the plateau regime.

Therefore, analyses in a collisionless regime are required in order to clarify the characteristics of GAM-like mode in the lower frequency range. It has been shown in this paper that geodesic currents have a maximum at a certain value of ω and changes sign in the low frequency range. These results will remain true even with the inclusion of a probable neoclassical polarization current. Therefore, there is a certain possibility that a new low frequency of GAM branch will be found in the collisionless (banana) regime with a damping rate smaller than that in the plateau regime.

VII. CONCLUSIONS

The geodesic mode was reconsidered in this paper in order to find some clues to understanding experimental observations of the GAM, which have different features depending on the device and operational parameter range: First, the role of the nonuniform potential field associated with the GAM was analyzed and its relation to coupling of GAMs with the two branches of sound waves were discussed. Specifically, coupling of the GAM with the ion acoustic wave was found to have strong effects in experiments carried out under the condition that the electron temperature is higher than that of ions. We therefore propose to measure the asymmetry of the potential for the clarification of this mechanism. In the present analyses, made avoiding the asymptotic expansions, it was found that there are typically two GAM frequencies: The one with higher frequency is the well-known GAM and the one found in the lower frequency range has been given little attention. The existence of the GAM in the low frequency range is attributed to the unique responses of the ions in this frequency range. The analyses with a full complex calculation showed that this mode has substantial damping. It is due to the rather strong dissipative response of ions in the low frequency range. It may, however, emerge as a well-defined mode in the treatment in a banana regime. The analyses developed in this paper allow inclusion of the multihelicity problem; in applications to toroidal helical systems, it was shown that helical devices have at least one tokamak-type GAM. It was found that a GAM of a purely helical nature occurs only under limited conditions ($T_e \gg 3T_i$); it emerges as the geodesic current is enhanced by the coupling with ion acoustic wave and has a strong helical asymmetry. In the systems of mixed helicity, the properties of the GAM changes from that of the tokamak type to that of the helical type as the helical geodesic curvature is increased.

ACKNOWLEDGMENTS

This paper is based on the material presented at the Second IAEA Technical Meeting on the Theory of Plasma Instabilities: Transport, Stability, and Their Interaction. The authors acknowledge stimulating discussions with Dr. T. S. Hahm, Dr. S. Sharapov, and Dr. B. Scott. T.W. thanks Dr. H. Sugama for useful discussions in revising the paper and Dr. B. J. Peterson for careful reading and grammatical advice.

This work was partly supported by the JSPS-Core University Program in the field of [Plasma and Nuclear Fusion].

APPENDIX: PROPERTIES OF THE DISPERSION FUNCTIONS

Three kinds of the dispersion functions Z_1,Z_2, and Z_p have been used in the main text. They differ in terms of the multiplicity with which the particle drift motion played a role:

$$Z_1 = \frac{1}{\sqrt{\pi}} \int \frac{1}{x-\zeta} \left((x)^4 + (x)^2 + \frac{1}{2} \right) \exp(-x^2) dx, \tag{A1}$$

$$Z_2 = \frac{1}{\sqrt{\pi}} \int \frac{1}{x-\zeta} \left(x^2 + \frac{1}{2} \right) \exp(-x^2) dx, \tag{A2}$$

$$Z_p = \frac{1}{\sqrt{\pi}} \int \frac{1}{x-\zeta} \exp(-x^2) dx. \tag{A3}$$

Here, their relationship and expansion formula are tabulated: Z_p is the well-known plasma dispersion function. Z_1 and Z_2 are expressed by using it as follows:

$$Z_1 = \zeta^3 + \frac{3}{2}\zeta + \left((\zeta)^4 + (\zeta)^2 + \frac{1}{2} \right) Z_p(\zeta), \tag{A4}$$

$$Z_2 = \zeta + \left(\zeta^2 + \frac{1}{2} \right) Z_p(\zeta). \tag{A5}$$

1. Asymptotic expansion

Asymptotic expansions of Z_1 and Z_2 are obtained from that of the plasma dispersion function Z_p:

$$Z_1 \approx -\left(\frac{7}{4}\frac{1}{\zeta} + \frac{23}{8}\frac{1}{\zeta^3} \right) + i\sqrt{\pi} \left((\zeta)^4 + (\zeta)^2 + \frac{1}{2} \right) \exp(-\zeta^2), \tag{A6}$$

$$Z_2 = -\left[\frac{1}{\zeta} + \left(\frac{1}{\zeta} \right)^3 \right] + i\sqrt{\pi} \left(\zeta^2 + \frac{1}{2} \right) \exp(-\zeta^2), \tag{A7}$$

$$Z_p \approx -\left(\frac{1}{\zeta} + \frac{1}{2}\frac{1}{\zeta^3} + \frac{3}{4}\frac{1}{\zeta^5} + \frac{15}{8}\frac{1}{\zeta^7} \right) + i\sqrt{\pi} \exp(-x^2). \tag{A8}$$

2. Series expansions

Series expansions of Z_1 and Z_2 are also obtained from that of the plasma dispersion function Z_p:

$$Z_1 \approx \frac{1}{2}\zeta - \frac{1}{3}\zeta^3 + i\sqrt{\pi}\left(\frac{1}{2} + \zeta^2 + \zeta^4\right)\exp(-\zeta^2), \tag{A9}$$

$$Z_2 \approx -\frac{4}{3}\zeta^3 + i\sqrt{\pi}\left(\frac{1}{2} + \zeta^2\right)\exp(-\zeta^2), \tag{A10}$$

$$Z_p \approx -\left(2\zeta - \frac{4}{3}\zeta^3\right) + i\sqrt{\pi}\exp(-x^2). \tag{A11}$$

These three dispersion functions are calculated and shown in Fig. 1 versus ζ. The most notable feature is that Z_1, the ion current caused by the uniform potential field, increases in proportion to $\zeta(\propto\omega)$ in the sense of polarization current in the low frequency range. This is quite different from the case of Z_p, where the current varies with the opposite coefficient of proportionality. It is also noted that Z_2 does not have a term proportional to ζ. These unique features of the geodesic response function originate from the multiplication factors in Eqs. (23) and (29).

[1] N. Winsor, J. L. Johnson, and J. M. Dawson, Phys. Fluids **11**, 2448 (1968).
[2] K. Hallatschek and D. Biskamp, Phys. Rev. Lett. **86**, 1223 (2001).
[3] B. N. Rogers and J. F. Drake, Phys. Rev. Lett. **79**, 229 (1997).
[4] B. N. Rogers, J. F. Drake, and A. Zeiler, Phys. Rev. Lett. **81**, 4396 (1998).
[5] A. Hasegawa and M. Mima, Phys. Fluids **21**, 87 (1978).
[6] A. Hasegawa and M. Wakatani, Phys. Rev. Lett. **59**, 1581 (1987).
[7] A. M. Dimits, T. J. Williams, J. A. Byers, and B. I. Chohen, Phys. Rev. Lett. **77**, 71 (1996).
[8] B. Scott, Phys. Plasmas **7**, 1845 (2000).
[9] T. S. Hahm, K. H. Burrel, Z. Lin, R. Nazikian, and E. J. Synakovskii, Plasma Phys. Controlled Fusion **42**, A205 (2000).
[10] M. Ramisch, U. Stroth, S. Niedner, and B. Scott, New J. Phys. **5**, 12.1 (2003).
[11] A. B. Hassam and J. F. Drake, Phys. Fluids B **5**, 4022 (1993).
[12] K. Itoh, K. Hallatschek, and S.-I. Itoh, Plasma Phys. Controlled Fusion **47**, 451 (2005).
[13] P. H. Diamond, S. Champeaux, M. Malkov *et al.*, Nucl. Fusion **41**, 1067 (2001).
[14] K. Itoh and S.-I. Itoh, Plasma Phys. Controlled Fusion **38**, 1 (1996).
[15] T. S. Hahm, M. A. Beer, Z. Lin, G. W. Hammett, W. W. Lee, and W. M. Tang, Phys. Plasmas **6**, 922 (1999).
[16] G. R. Mackee, R. J. Fonck, M. Jakubowski, K. H. Burrell, K. Hallastschek, R. A. Moyer, W. Nevins, D. L. Rudakov, and X. Xu, Plasma Phys. Controlled Fusion **45**, A477 (2003).
[17] P. M. Schoch, K. A. Conner, D. R. Demers, and X. Zhang, Rev. Sci. Instrum. **74**, 1846 (2003).
[18] Y. W. Tsui, P. M. Schoch, and A. J. Wootton, Phys. Fluids B **5**, 1274 (1993).
[19] Y. Hamada, A. Nishizawa, T. Ido, T. Watari, M. Kojima, K. Kawasumi, K. Narihara, K. Toi, and JIPP T-IIU Group, Nucl. Fusion **45**, 81 (2005).
[20] Y. Hamada, N. Nishizawa, Y. Kawasumi, A. Fujisawa, H. Iguchi, and JIPP T-IIU group, Fusion Eng. Des. **34–35**, 663 (1997).
[21] T. Ido, Y. Miura, K. Kamiya, Y. Hamada, K. Hoshino, A. Fujisawa, K. Itoh, S.-I. Itoh, A. Nishizawa, H. Ogawa, Y. Kusama, and JFT-2M group, Plasma Phys. Controlled Fusion **48**, 41 (2006).
[22] A. Fujisawa, K. Itoh, H. Iguchi *et al.*, Phys. Rev. Lett. **93**, 165002 (2004).
[23] M. G. Shats and W. M. Solomon, Phys. Rev. Lett. **88**, 045001 (2002).
[24] G. S. Xu, B. N. Wan, M. Song, and J. Li, Phys. Rev. Lett. **91**, 125001 (2003).
[25] G. D. Conway, B. Scott, J. Schirmer, M. Reich, A. Kendl, and ASDEX Upgrade Team, Plasma Phys. Controlled Fusion **47**, 1165 (2005).
[26] A. V. Melnikov, V. A. Vershkov, L. G. Eliseev, S. A. Grashin, *et al.*, Plasma Phys. Controlled Fusion **48**, 87 (2006).
[27] P. H. Diamond, S.-I. Itoh, K. Itoh, and T. S. Hahm, Plasma Phys. Controlled Fusion **47**, R35 (2005).
[28] T. S. Hahm, Plasma Phys. Controlled Fusion **44**, A87 (2002).
[29] S. V. Novakovskii, C. S. Liu, R. Z. Sagdeef, and M. N. Rosenbluth, Phys. Plasmas **4**, 4272 (1997).
[30] M. N. Rosenbluth and F. L. Hinton, Phys. Rev. Lett. **80**, 724 (1998).
[31] F. L. Hinton and M. N. Rosenbluth, Plasma Phys. Controlled Fusion **41**, A653 (1999).
[32] T. Watari, Y. Hamada, A. Fujisawa, K. Toi, K. Itoh, Phys. Plasmas **12**, 062304, 2005.
[33] T. Watari, Y. Hamada, A. Nishizawa, J. Todoroki, and K. Itoh, "Unified linear response functions in the zonal flow to geodesic acoustic mode frequency range," (presented at the International Tokamak Physics Activity Meeting, Kyoto, April, 2005) (NIFS-815, Sept. 2005; internal report in NIFS available at http://www.nifs.ac.jp/report/index.html).
[34] V. B. Lebedev, P. N. Yushumanov, P. H. Diamond, S. V. Novakovskii, and A. I. Smoliakov, Phys. Plasmas **3**, 3203 (1996).
[35] H. Sugama and T. H. Watanabe, Phys. Plasmas **13**, 012501 (2006).
[36] S. Satake, M. Okamoto, N. Nakajima *et al.*, Nucl. Fusion **45**, 1362 (2005).